

## Identification of Protein-Bound Dinitrosyl Iron Complexes by Nuclear Resonance Vibrational Spectroscopy

Zachary J. Tonzetich,<sup>†</sup> Hongxin Wang,<sup>‡</sup> Devrani Mitra,<sup>||</sup> Christine E. Tinberg,<sup>†</sup>  
Loi H. Do,<sup>†</sup> Francis E. Jenney, Jr.,<sup>§</sup> Michael W. W. Adams,<sup>#</sup> Stephen P. Cramer,<sup>\*,||,‡</sup> and  
Stephen J. Lippard<sup>\*,†</sup>

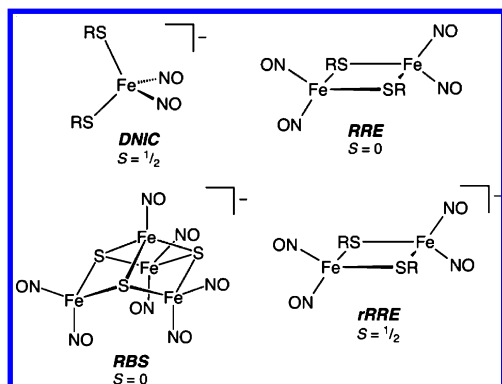
Department of Chemistry, Massachusetts Institute of Technology, Cambridge, Massachusetts 02139, Department of Applied Science, University of California, Davis, California 95616, Physical Biosciences Division, Lawrence Berkeley National Laboratory, Berkeley, California 94720, GA Campus—Philadelphia College of Osteopathic Medicine, Suwanee, Georgia 30024, and Department of Biochemistry and Molecular Biology, University of Georgia, Athens, Georgia 30602

Received February 4, 2010; E-mail: spcramer@lbl.gov; lippard@mit.edu

Among various sites of nitric oxide reactivity in biology,<sup>1</sup> iron–sulfur clusters have emerged as an important class of metallocofactors targeted by NO.<sup>2</sup> Proteins containing these clusters perform a diverse array of functions from electron transfer to small molecule sensing and substrate binding.<sup>3</sup> Consequently, iron–sulfur clusters are potential sites for both NO-derived physiological signal transduction<sup>4</sup> and toxicity.<sup>2a,5</sup>

The primary products of NO reactivity at iron–sulfur clusters are dinitrosyl iron complexes (DNICs).<sup>6</sup> Identification of DNICs in proteins and tissue samples has traditionally relied upon the diagnostic  $g = 2.03$  EPR signal,<sup>7</sup> which is characteristic of these  $S = 1/2$  species. Because iron dinitrosyl complexes can exist in forms other than the paramagnetic mononuclear species (Chart 1), however, EPR characterization is not definitive.<sup>8</sup> Other means of characterization include <sup>57</sup>Fe Mössbauer,<sup>9</sup> UV–vis,<sup>10</sup> Raman,<sup>11</sup> and X-ray absorption spectroscopy,<sup>12</sup> but each of these techniques lacks diagnostic spectroscopic markers and cannot easily deconvolute spectra resulting from a mixture of species.

**Chart 1.** Examples of Sulfur-Ligated Iron Dinitrosyls



In order to overcome these challenges, we have utilized <sup>57</sup>Fe nuclear resonance vibrational spectroscopy (NRVS) to characterize the core vibrations of several iron dinitrosyl complexes. This technique is selective for motion of the <sup>57</sup>Fe nucleus, making it an ideal means of probing DNICs in protein environments.<sup>13</sup> NRVS is not limited by the selection rules of infrared and Raman spectroscopy, ensuring that a complete set of vibrational modes

involving motion of the <sup>57</sup>Fe nucleus is observed. Here we present the first NRVS results for a nitrosylated iron–sulfur cluster protein, as well as complementary data on several biomimetic model compounds. The detection of RBS (Chart 1) upon nitrosylation of the protein demonstrates the power of the methodology.

In order to provide spectroscopic benchmarks to identify DNICs in proteins, we investigated synthetic analogues comprising the four structures displayed in Chart 1. To provide maximum NRVS signal intensity, the model compounds were prepared from <sup>57</sup>Fe-enriched Fe(OTf)<sub>2</sub>·2CH<sub>3</sub>CN (see Supporting Information (SI) for experimental details). The benzene thiolate ligand (Chart 1, R = Ph) was chosen because it facilitates the synthesis and isolation of the different <sup>57</sup>Fe-labeled derivatives and because the NRVS spectrum of the related Fe–S cluster, [Fe<sub>4</sub>S<sub>4</sub>(SPh)<sub>4</sub>]<sup>2-</sup>, was recorded previously.<sup>14</sup> Additionally, (Et<sub>4</sub>N)[Fe(NO)<sub>2</sub>(SPh)<sub>2</sub>], [Fe<sub>2</sub>(μ-SPh)<sub>2</sub>(NO)<sub>4</sub>] (Roussin's red ester, RRE), and (Et<sub>4</sub>N)-[Fe<sub>4</sub>S<sub>3</sub>(NO)<sub>7</sub>] (Roussin's black salt, RBS) were prepared using both <sup>14</sup>NO and <sup>15</sup>NO to help identify normal modes involving the nitrosyl ligands.

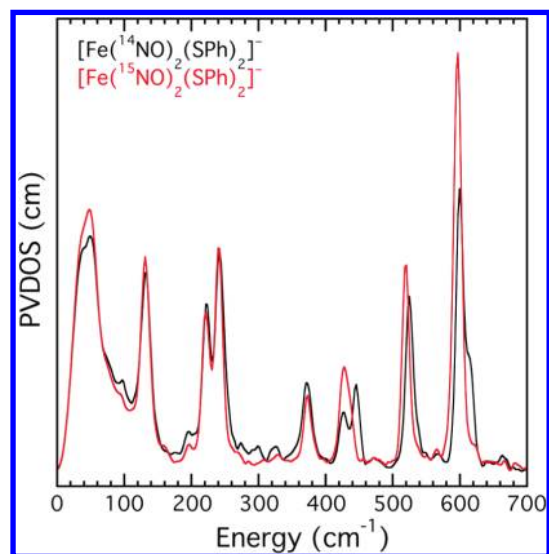


**Figure 1.** <sup>57</sup>Fe partial vibrational density of states (PVDOS) for (Et<sub>4</sub>N)[Fe(NO)<sub>2</sub>(SPh)<sub>2</sub>].

A representative NRVS spectrum of one of the model compounds, (Et<sub>4</sub>N)[Fe(<sup>14/15</sup>NO)<sub>2</sub>(SPh)<sub>2</sub>], is shown in Figure 1. Of note are the intense peaks above 500 cm<sup>-1</sup>, which shift to lower energy upon <sup>15</sup>N substitution. The NRVS spectra of [Fe<sub>2</sub>(μ-SPh)<sub>2</sub>(<sup>14/15</sup>NO)<sub>4</sub>]

<sup>†</sup> Massachusetts Institute of Technology.

<sup>||</sup> University of California, Davis.

<sup>‡</sup> Lawrence Berkeley National Laboratory.

<sup>§</sup> GA Campus—Philadelphia College of Osteopathic Medicine.

<sup>#</sup> University of Georgia.

and  $(\text{Et}_4\text{N})[\text{Fe}_4\text{S}_3(^{14/15}\text{NO})_7]$  display similarly shifted peaks (Figures S17–S19), indicating that vibrations in this region most likely originate from the symmetric and asymmetric stretching modes of the N–Fe–N unit.<sup>11</sup> In all four model compounds, the peak near  $600\text{ cm}^{-1}$  appears to contain a higher energy shoulder (e.g., Figure 1). We assign this feature to Fermi resonance on the basis of the calculated spectrum for each model compound (see SI) and its disappearance upon  $^{15}\text{N}$  substitution (Figure 1). Despite this minor complexity, the region of the spectrum between  $500$  and  $700\text{ cm}^{-1}$  provides important diagnostic NRVS signatures for each of the iron dinitrosyl species displayed in Chart 1 (Figure S20, SI). Furthermore, the vibrations occur in a region of the spectrum that does not overlap with normal modes due to thiolate ligands or the  $\{\text{Fe}_4\text{S}_4\}$  core, thereby providing clear information about the nature of the Fe–NO species present. EPR spectroscopy fails in this regard because the RRE and RBS compounds are diamagnetic, and  $^{57}\text{Fe}$  Mössbauer spectroscopy is complicated by the fact that isomer shifts for all four dinitrosyl-containing species are very similar (Figure S25 and Table S2, SI).

For protein studies, a ferredoxin D14C variant from *Pyrococcus furiosus* was selected as a model system because of its stability at high concentrations (mM) and relatively solvent-exposed  $\text{Fe}_4\text{S}_4$  cluster (Figure S26, SI).<sup>15</sup> In the native form of the protein, the iron–sulfur cluster is bound by one aspartate (D14) and three cysteinate residues. For the present purposes, a D14C mutant was examined because it provides a more representative model of  $\text{Fe}_4\text{S}_4$  clusters, which typically have four terminal cysteine thiolate ligands. Moreover, NRVS data on the untreated D14C mutant were already available,<sup>16</sup> affording an opportunity to distinguish vibrations of the unmodified protein from those of the NO reaction product(s) (Figure S28, SI).

Reaction of *P. furiosus* ferredoxin with the nitric oxide donor PAPA NONOate gave rise to a single  $g_{\text{av}} = 2.03$  EPR signal characteristic of a protein-bound DNIC (Figure S27, SI). EPR spectroscopy provided no evidence for formation of rRRE ( $g_{\text{av}} = 1.99$ ),<sup>17</sup> and spin quantitation of the DNIC signal revealed that this species accounted for only about 5–10% of the total protein concentration. Examination of the reaction mixture by NRVS, however, indicated significant formation of an iron dinitrosyl (Figure 2 and Figure S28, SI). The spectral features of this species were inconsistent with either the DNIC or the diamagnetic RRE. By comparison with the model compounds, we assign this product as the tetranuclear RBS ( $[\text{Fe}_4\text{S}_3(\text{NO})_7]^-$ , Chart 1).

Formation of RBS by nitrosylation of a protein-bound  $\text{Fe}_4\text{S}_4$  cluster has not been previously reported, although reactions of a variety of synthetic  $\text{Fe}_4\text{S}_4$  clusters with NO gas generate the black salt.<sup>18</sup> RBS formation may be related to the highly solvent-exposed nature of the  $\text{Fe}_4\text{S}_4$  cluster in *P. furiosus* Fd, but further work is required to test this possibility as well as its potential generality. The formation of RBS, however, could help explain the results obtained in reactions of other  $\text{Fe}_4\text{S}_4$  cluster proteins with NO, where EPR spin quantitation of protein-bound DNICs accounts for only a fraction of the total iron content.<sup>19</sup>

Roussin's black salt is toxic to cells,<sup>2a,20</sup> and its formation from Fe–S clusters is a plausible mode of NO-derived toxicity in vivo. Our data provide the first evidence for the direct formation of this species from an iron–sulfur protein. The presence of RBS in addition to DNICs may have important implications for the repair of nitrosylated iron–sulfur clusters,<sup>21</sup> the mechanism of NO signal transduction, and other biological consequences of nitric oxide chemistry at iron–sulfur protein cores.

In conclusion, we provide here the first NRVS spectra of non-heme iron nitrosyl compounds and demonstrate the value of this

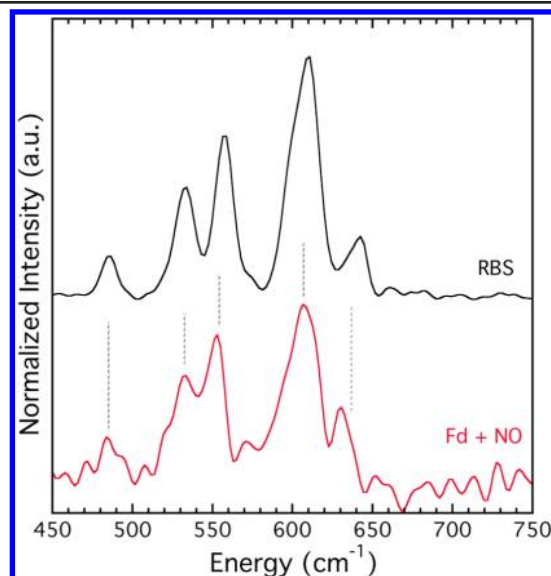


**Figure 2.** Comparison of the NRVS spectrum of RBS and the spectrum resulting from treatment of  $^{57}\text{Fe}$ -enriched *P. furiosus* Fd D14C with PAPA NONOate.

technique in identifying the products of iron–sulfur cluster nitrosylation. In particular, the method has proved valuable in identifying diamagnetic dinitrosyl iron species that would otherwise be very difficult to observe. Moving forward, we envision extending these studies to identify the products of other biological NO targets and to help define the roles of nitric oxide in modulating the functions of non-heme iron proteins.

**Acknowledgment.** This work was funded by grants from the NSF (CHE-0611944 to S.J.L. and CHE-07453535 to S.P.C.), the NIH (GM65440 to S.P.C.), and the DOE (DE-FG02-05ER15710 to M.W.A.). Z.J.T. thanks NIGMS for a postdoctoral fellowship (1 F32 GM082031-02). C.E.T. received partial support under Interdepartmental Training Grant T32 GM08334 from NIGMS. NRVS spectra were measured at Spring-8 BL09XU with the approval of JASRI (Proposal No. 2009A0015) and the help of Dr. Yoshitaka Yoda. The beamline BL09XU was upgraded with the JST (CREST) fund. We also thank Dr. Ilya Sergeev (ESRF) for help with the NRVS of rRRE.

**Supporting Information Available:** Experimental procedures, additional figures, crystallographic data collection and refinement details, and fully labeled thermal ellipsoid diagrams for  $[\text{Fe}_2(\mu\text{-SPH})_2(\text{NO})_4]$  and  $(\text{Et}_4\text{N})[\text{Fe}_2(\mu\text{-SPH})_2(\text{NO})_4]$ , as well as the corresponding CIF files. This information is available free of charge via the Internet at <http://pubs.acs.org>.

## References

- (1) (a) *Nitric Oxide: Biology and Pathobiology*; Ignarro, L. J., Ed.; Academic Press: San Diego, 2000. (b) McCleverty, J. A. *Chem. Rev.* **2004**, *104*, 403–418.
- (2) (a) Butler, A. R.; Megson, I. L. *Chem. Rev.* **2002**, *102*, 1155–1165. (b) Szaciłowski, K.; Chmura, A.; Stasicka, Z. *Coord. Chem. Rev.* **2005**, *249*, 2408–2436.
- (3) Beinert, H.; Holm, R. H.; Münck, E. *Science* **1997**, *277*, 653–659.
- (4) Ding, H.; Demple, B. *Proc. Natl. Acad. Sci. U.S.A.* **2000**, *97*, 5146–5150.
- (5) Asanuma, K.; Iijima, K.; Ara, N.; Koike, T.; Yoshitake, J.; Ohara, S.; Shimosegawa, T.; Yoshimura, T. *Nitric Oxide* **2007**, *16*, 395–402.
- (6) Reddy, D.; Lancaster, J. R., Jr.; Cornforth, D. P. *Science* **1983**, *221*, 769–770.
- (7) Vanin, A. F.; Serezhnikov, V. A.; Mikoyan, V. D.; Genkin, M. V. *Nitric Oxide* **1998**, *2*, 224–234.
- (8) Butler, A. R.; Glidewell, C.; Li, M.-H. *Adv. Inorg. Chem.* **1988**, *32*, 335–393.
- (9) Lobysheva, I. I.; Serezhnikov, V. A.; Stucan, R. A.; Bowman, M. K.; Vanin, A. F. *Biochemistry (Moscow)* **1997**, *62*, 801–808.

- (10) Foster, M. W.; Cowan, J. A. *J. Am. Chem. Soc.* **1999**, *121*, 4093–4100.
- (11) Dai, R. J.; Ke, S. C. *J. Phys. Chem. B* **2007**, *111*, 2335–2346.
- (12) Tsai, M.-C.; Tsai, F.-T.; Lu, T.-T.; Tsai, M.-L.; Wei, Y.-C.; Hsu, I.-J.; Lee, J.-F.; Liaw, W.-F. *Inorg. Chem.* **2009**, *48*, 9579–9591.
- (13) Scheidt, W. R.; Durbin, S. M.; Sage, J. T. *J. Inorg. Biochem.* **2005**, *99*, 60–71.
- (14) Xiao, Y.; Koutmos, M.; Case, D. A.; Coucouvanis, D.; Wang, H.; Cramer, S. P. *Dalton Trans.* **2006**, 2192–2201.
- (15) Aono, S.; Bryant, F. O.; Adams, M. W. W. *J. Bacteriol.* **1989**, *171*, 3433–3439.
- (16) Cramer, S. P.; Xiao, Y.; Wang, H.; Guo, Y.; Smith, M. C. *Hyperfine Interact.* **2006**, *170*, 47–54.
- (17) Lu, T.-T.; Tsou, C.-C.; Huang, H.-W.; Hsu, I.-J.; Chen, J.-M.; Kuo, T.-S.; Wang, Y.; Liaw, W.-F. *Inorg. Chem.* **2008**, *47*, 6040–6050.
- (18) Harrop, T. C.; Tonzetich, Z. J.; Reisner, E.; Lippard, S. J. *J. Am. Chem. Soc.* **2008**, *130*, 15602–15610.
- (19) (a) Kennedy, M. C.; Antholine, W. E.; Beinert, H. *J. Biol. Chem.* **1997**, *272*, 20340–20347. (b) Cruz-Ramos, H.; Crack, J.; Wu, G.; Hughes, M. N.; Scott, C.; Thomson, A. J.; Green, J.; Poole, R. K. *EMBO J.* **2002**, *21*, 3235–3244. (c) Yukl, E. T.; Elbaz, M. A.; Nakano, M. M.; Moënne-Loccoz, P. *Biochemistry* **2008**, *47*, 13084–13092.
- (20) Hamilton-Brehm, S. D.; Schut, G. J.; Adams, M. W. W. *Appl. Environ. Microbiol.* **2009**, *75*, 1820–1825.
- (21) (a) Rogers, P. A.; Eide, L.; Klungland, A.; Ding, H. *DNA Repair* **2003**, *2*, 809–817. (b) Tsou, C.-C.; Lin, Z.-S.; Lu, T.-T.; Liaw, W.-F. *J. Am. Chem. Soc.* **2008**, *130*, 17154–17160.

JA101002F